Supplementary Information: Fermat's Spiral-Based Characterization of Squeezed Nonlinear Motional States of Levitated Nanoparticle

Martin Duchaň,[1,*] Alexandr Jonáš,[1] Radim Filip,[2] Jan Ježek,[1] Petr Jákl,[1] Pavel Zemánek,[1] and Martin Šiler[1,†]

[1] *Institute of Scientific Instruments of the Czech Academy of Sciences, Královopolská 147, 612 64 Brno, Czech Republic*

[2] *Department of Optics, Palacký University, 17. listopadu 1192/12, 771 46 Olomouc, Czech Republic*

S1. DYNAMICS OF PARTICLE MOTION IN HARMONIC-LIKE POTENTIALS

Let us assume a spherical particle of radius a and mass m moving in a viscous medium characterized by temperature T. In principle, the evolution of a single stochastic realization of the particle trajectory may be characterized by Langevin equations

$$\dot{z}(t) = v(t), \tag{S1}$$

$$\dot{v}(t) = \frac{1}{m}F(z) - \Gamma v(t) + \eta_{\mathrm{r}}(t), \tag{S2}$$

where $z(t)$ is the particle position and $v(t)$ is the particle velocity. The forces that affect the motion of the particle, appearing on the right-hand side of Eq. (S2), are

1. External position-dependent force $F(z)$ that can be realized, for example, by optical trapping [1] or by the (quasi-)static electric fields in the so-called Paul trap [2]. Here, we focus on two particular types of force fields:

   (a) Harmonic restoring force corresponding to a linear spring with a stiffness κ, leading to periodic oscillations of the particle in a parabolic potential

   $$F(z) = -\kappa z + F_{\mathrm{c}} \equiv -m\Omega_0^2 z + F_{\mathrm{c}}, \tag{S3}$$

   where $\Omega_0 = \sqrt{\kappa/m}$ denotes the characteristic frequency of particle's oscillations. F_{c} is then an additional constant force that effectively shifts the equilibrium position of the particle in the parabolic potential.

   (b) Destabilizing linear force

   $$F(z) = +\kappa_{\mathrm{i}} z + F_{\mathrm{c}} \equiv +m\Omega_{\mathrm{i}}^2 z + F_{\mathrm{c}}, \tag{S4}$$

   where Ω_{i} denotes an effective frequency corresponding to a harmonic-like force of the stiffness $-\kappa_i$. Formally, Eq. (S4) corresponds to Eq. (S3) upon the substitution $\Omega_0 = \mathrm{i}\Omega_{\mathrm{i}}$.

   The above-considered forces, Eqs. (S3) and (S4), which can be mutually combined, always result in linear dynamics of the nanoparticle, described by the linear ordinary differential equations of motion, (S1) and (S2).

2. Velocity-dependent viscous damping force $-m\Gamma v(t)$ proportional to the damping rate Γ. For a particle immersed in a liquid, the damping rate is $\Gamma = \gamma/m = 6\pi\nu a/m$, with γ being the Stokes drag coefficient and ν being the dynamic viscosity of the liquid. Experiments analyzed in this article were carried out in a rarefied gaseous atmosphere, under the conditions of partial vacuum. At these low pressures, an additional dependence of Γ on the ambient pressure appears that follows [3]

   $$\Gamma = \frac{6\pi\nu a}{m}\left(\frac{0.619}{0.619+\mathrm{Kn}}\right)\left(1+\frac{0.31\mathrm{Kn}}{0.785+1.152\mathrm{Kn}+\mathrm{Kn}^2}\right), \tag{S5}$$

   where Kn is the Knudsen number, defined as the ratio of the pressure-dependent mean free path of the gas molecules and the radius of the particle. The full original formula for Γ that also takes into account various types of energy and momentum accommodation is given in [4]. For the actual experimental values of the relevant parameters (particle radius 150 nm, particle density $\rho = 2000$ kg.m^{-3}, and ambient air pressure 1 mbar), we obtained the value of $\Gamma/(2\pi) = 0.39\,\mathrm{kHz}$.

* duchan@isibrno.cz
† siler@isibrno.cz

3. Stochastic force caused by the collisions of the gas molecules with the particle. It can be described by the random process $\eta_\mathrm{r}(t)$ (white noise) that has zero mean and time correlation given by

$$\langle \eta_\mathrm{r}(t)\eta_\mathrm{r}(t')\rangle = \frac{2k_\mathrm{B}T\Gamma}{m}\delta(t-t'),$$

where k_B is the Boltzmann constant and $\delta(t)$ is Dirac's delta function.

The probability density function (PDF) $P(z,v,t)$ that corresponds to the random process described by the Langevin Eqs. (S1) and (S2) can be obtained by solving the Fokker-Planck equation

$$\frac{\partial P}{\partial t} = -\frac{\partial}{\partial z}vP + \frac{\partial}{\partial v}\left[\Gamma v - \frac{F(z)}{m}\right]P + \Gamma\frac{k_B T}{m}\frac{\partial^2}{\partial v^2}P, \tag{S6}$$

for details see [5]. When the initial PDF at time $t=0$ is Gaussian, the solution of Eq. (S6) will be a Gaussian function as well, as long as the force $F(z)$ acting on the particle has the general linear form of Eqs. (S3) and (S4). Such time-dependent Gaussian PDF is fully described by its mean values and elements of the covariance matrix, namely, the means and variances of position z and velocity v and the covariance of z and v.

The initial Gaussian PDF in the phase space is given by

$$P_0(\boldsymbol{z}) = \frac{1}{2\pi\sqrt{\det\boldsymbol{\Theta}_0}}\exp\left\{-\frac{1}{2}\left[\boldsymbol{z}-\boldsymbol{\mu}_0\right]^\mathrm{T}\boldsymbol{\Theta}_0^{-1}\left[\boldsymbol{z}-\boldsymbol{\mu}_0\right]\right\}, \tag{S7}$$

where $^\mathrm{T}$ denotes transposition,

$$\boldsymbol{z} = \begin{pmatrix} z \\ v \end{pmatrix} \quad \text{and} \quad \boldsymbol{\mu}_0 = \begin{pmatrix} \mu_{0,z} \\ \mu_{0,v} \end{pmatrix}$$

are the column vector of the phase-space position and velocity and the column vector of the initial mean values of position and velocity, respectively, and the initial covariance matrix $\boldsymbol{\Theta}_0$ of the position and velocity variables is

$$\boldsymbol{\Theta}_0 = \begin{pmatrix} \theta_{0zz} & \theta_{0zv} \\ \theta_{0vz} & \theta_{0vv} \end{pmatrix}. \tag{S8}$$

Note that in the following text, we will use symbols θ_0 to describe the elements of the initial covariance matrix $\boldsymbol{\Theta}_0$ at time $t=0$, while $\theta(t)$ denotes the elements of the covariance matrix at a given time $t>0$.

S1.1. Normalized coordinates

For the sake of clarity, it is useful to introduce dimensionless phase-space coordinates instead of the physical coordinates (z,v), and replace the physical time t with normalized time. As normalization factors for the phase-space coordinates, we employ the initial standard deviations of z and v corresponding to the effective initial temperature T_0 of the particle, which could be different from the ambient temperature T due to active cooling of the particle motion [3]. The time can then be naturally normalized using the characteristic oscillation frequency of the trapping potential, Ω_0. Using these conventions, the dimensionless phase-space coordinates $(\bar{z},\bar{v})$ and the dimensionless time $\bar{t}$ are

$$\bar{z} = \sqrt{\frac{m\Omega_0^2}{k_\mathrm{B}T_0}}z, \tag{S9}$$

$$\bar{v} = \sqrt{\frac{m}{k_\mathrm{B}T_0}}v, \tag{S10}$$

$$\bar{t} = \Omega_0 t. \tag{S11}$$

In principle, the position coordinate is normalized to the standard deviation of particle position in the harmonic trap with restoring frequency Ω_0. Similarly, the velocity coordinate is normalized by the root-mean-square velocity of the particle given by the Maxwell-Boltzmann distribution of particle velocities. In the following text, we will denote the dimensionless coordinates and all related quantities derived from them by over-bars.

Following the normalization procedure of Eqs. (S9) and (S10), the parameters of the Gaussian PDF in the normalized coordinates are given as

$$\bar{\theta}_{zz}(\bar{t}) = \frac{m\Omega_0^2}{k_\mathrm{B}T_0}\theta_{zz}(\bar{t}), \qquad \bar{\theta}_{vv}(\bar{t}) = \frac{m}{k_\mathrm{B}T_0}\theta_{vv}(\bar{t}), \qquad \bar{\theta}_{zv}(\bar{t}) = \bar{\theta}_{vz}(\bar{t}) = \frac{m\Omega_0}{k_\mathrm{B}T_0}\theta_{zv}(\bar{t}), \tag{S12}$$

$$\bar{\mu}_z(\bar{t}) = \sqrt{\frac{m\Omega_0^2}{k_\mathrm{B}T_0}}\mu_z(\bar{t}), \qquad \bar{\mu}_v(\bar{t}) = \sqrt{\frac{m}{k_\mathrm{B}T_0}}\mu_v(\bar{t}). \tag{S13}$$

Therefore, the normalized covariance matrix is

$$\bar{\mathbf{\Theta}}(\bar{t}) = \begin{pmatrix} \bar{\theta}_{zz}(\bar{t}) & \bar{\theta}_{zv}(\bar{t}) \\ \bar{\theta}_{zv}(\bar{t}) & \bar{\theta}_{vv}(\bar{t}) \end{pmatrix} = \frac{m}{k_\mathrm{B}T_0}\begin{pmatrix} \Omega_0^2\,\theta_{zz}(\bar{t}) & \Omega_0\,\theta_{zv}(\bar{t}) \\ \Omega_0\,\theta_{zv}(\bar{t}) & \theta_{vv}(\bar{t}) \end{pmatrix}. \tag{S14}$$

The normalization adopted above guarantees that the covariance matrix corresponding to the state of thermal equilibrium at temperature T_0 is a unit matrix.

S1.2. Gaussian state evolution

The time evolution of the PDF is given by the convolution of the PDF (S7) of the initial state with the phase-space trajectory of the system described by Eqs. (S1) and (S2) that starts from a single initial point. The result of this convolution may be formally written as [6, 7]

$$P(\bar{\boldsymbol{z}}, \bar{t}|\bar{\boldsymbol{\mu}}(\bar{t}), \bar{\mathbf{\Theta}}(\bar{t})) = \frac{1}{2\pi\sqrt{\det\bar{\mathbf{\Theta}}(\bar{t})}}\exp\left\{-\frac{1}{2}\left[\bar{\boldsymbol{z}} - \bar{\boldsymbol{\mu}}(\bar{t})\right]^\mathrm{T}\bar{\mathbf{\Theta}}(\bar{t})^{-1}\left[\bar{\boldsymbol{z}} - \bar{\boldsymbol{\mu}}(\bar{t})\right]\right\}. \tag{S15}$$

Vector $\bar{\boldsymbol{\mu}}(\bar{t})$ that describes the actual time-dependent mean values of the state evolves as

$$\bar{\boldsymbol{\mu}}(\bar{t}) = \bar{\mathbf{U}}(\bar{t})\bar{\boldsymbol{\mu}}_\mathbf{0} + \bar{\boldsymbol{u}}(\bar{t}). \tag{S16}$$

Here, $\bar{\mathbf{U}}(\bar{t})$ is a 2×2 matrix describing the transient evolution of the system exposed to an external force $F(z)$ (see details below) and $\bar{\boldsymbol{u}}(\bar{t})$ is a particular solution of the Langevin equation in the cases for which $F_\mathrm{c} \neq 0$. Furthermore, the time-dependent covariance matrix

$$\bar{\mathbf{\Theta}}(\bar{t}) = \bar{\mathbf{\Theta}}_\mathrm{D}(\bar{t}) + \bar{\mathbf{U}}(\bar{t})\bar{\mathbf{\Theta}}_\mathbf{0}\bar{\mathbf{U}}^T(\bar{t}) \tag{S17}$$

can be decomposed into two terms. The first term, $\bar{\mathbf{\Theta}}_\mathbf{D}(\bar{t})$, reflects the system's diffusive approach to thermal equilibrium, which gradually dominates in the final state, while the second term, $\bar{\mathbf{U}}(\bar{t})\bar{\mathbf{\Theta}}_\mathbf{0}\bar{\mathbf{U}}^T(\bar{t})$, captures the transient influence of the initial state that diminishes over time.

The specific form of the evolution matrix $\bar{\mathbf{U}}(\bar{t})$ represents the particular external force $F(z)$ associated with a potential profile in which the particle moves, see Fig. S1. This evolution can be viewed as a linear operation on the state and determines how the mean values and covariance matrix of the state evolve over time, as described in Eqs. (S16) and (S17). A sequence of different potentials can be applied to the particle, allowing a series of operations to be performed on its state. The effect of a particular potential applied to the particle over a period of time $\bar{t}$ is fully described by the corresponding forms of $\bar{\mathbf{U}}(\bar{t})$, $\bar{\boldsymbol{u}}(\bar{t})$, and $\bar{\mathbf{\Theta}}_\mathbf{D}(\bar{t})$. Consequently, any sequence of operations can be represented as multiplication and summation of matrices characterizing these operations. The elements of the matrices are functions of time $\bar{t}$ spent by the particle in the particular potential, so it always holds $\bar{t} \geq 0$. The full expressions for the matrix elements in various scenarios are provided in the SI of Ref. [7].

In the following text, we will present equations for $\bar{\mathbf{U}}(\bar{t})$, $\bar{\boldsymbol{u}}(\bar{t})$, and $\bar{\mathbf{\Theta}}_\mathrm{D}(\bar{t})$ in three cases that may be used to create any desired initial Gaussian state. Namely, we consider the evolution in

a. The *parabolic trapping potential* (PP) with the trap frequency Ω_0, i.e., the same frequency as used in the coordinate normalization,

b. The *weak parabolic potential* (WPP) with the trap frequency $\Omega_\mathrm{w} \neq \Omega_0$ and the overall force that is still restoring. We use the term "weak" here as the frequencies $0 \leq \Omega_\mathrm{w} < \Omega_0$ are more readily experimentally available, but the description is valid also for $\Omega_\mathrm{w} > \Omega_0$.

c. The *inverted parabolic potential* (IPP) that results from the destabilizing linear force (S4) and may be characterized by the effective frequency Ω_i.

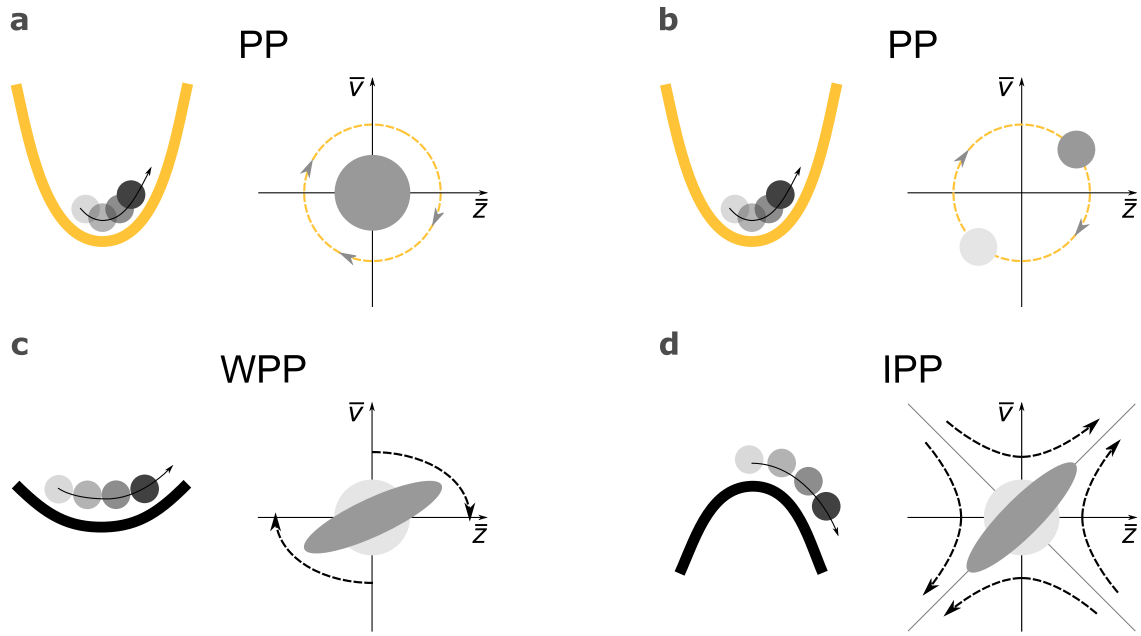

Figure S1. **Illustration of linear operations experimentally performed on an initial state in the phase space** $(\bar{z}, \bar{v})$ **for** $\Gamma = 0$**.** In a parabolic potential (PP), the state rotates (a) or orbits (b) in the phase space without changing shape. (c) Squeezing/extension of the state, accompanied by state rotation, is realized using a weak parabolic potential (WPP). (d) Squeezing/extension of the state, accompanied by additional displacement (not depicted), is realized using an inverted parabolic potential (IPP). The actual experimental implementation of individual potentials using standing-wave optical trapping is described in section S3.

In all cases considered in the following text, we will assume weak damping, i.e. $\Gamma \ll \Omega_0$, and also $\Gamma\bar{t}/\Omega_0 \ll 1$. Therefore, in the treatment of diffusive behavior, we will approximate exponential functions of the form $\exp(-\Gamma\bar{t}/\Omega_0)$ by their Taylor-series expansions. The full description of the state evolution without any approximations can be found in the SI of [7].

a. Parabolic trapping potential (PP). The evolution of the state in the confining PP with the characteristic frequency Ω_0 corresponds to the rotation of the state in the phase space with the same frequency. The evolution matrices are given by

$$\bar{\mathbf{U}}_{\mathrm{PP}}(\bar{t}) = \left(1 - \frac{\Gamma\bar{t}}{2\Omega_0}\right) \begin{pmatrix} \cos\bar{t} & \sin\bar{t} \\ -\sin\bar{t} & \cos\bar{t} \end{pmatrix}, \tag{S18}$$

$$\bar{\mathbf{\Theta}}_{\mathrm{D,PP}}(\bar{t}) = \frac{T\Gamma}{T_0\Omega_0} \begin{pmatrix} \bar{t}\,(1 - \operatorname{sinc} 2\bar{t}) & \sin^2\bar{t} \\ \sin^2\bar{t} & \bar{t}\,(1 + \operatorname{sinc} 2\bar{t}) \end{pmatrix}. \tag{S19}$$

Figure S1(a,b) illustrates the time evolution of the state in the PP. If the particle is initially in thermal equilibrium with the ambient atmosphere, its state remains unchanged during the evolution (panel a). In contrast, the state that is initially displaced from the phase-space origin orbits around the origin. In the ideal case without damping, the orbit is stable (part b), whereas for the realistic case of non-zero damping, the state spirals towards the origin, gradually thermalizing with the environment.

b. Weak parabolic potential (WPP). The evolution in a WPP generally causes squeezing and extension of the state in the phase space. The strength of this state operation then depends on the ratio of the characteristic frequencies of the original trapping potential, Ω_0, and the weakened potential, $\Omega_{\rm w} < \Omega_0$. The evolution matrices are given by

$$\bar{\mathbf{U}}_{\rm WPP}(\bar{t}) = \left(1 - \frac{\Gamma\bar{t}}{2\Omega_0}\right) \begin{pmatrix} \cos\frac{\Omega_{\rm w}}{\Omega_0}\bar{t} & \frac{\Omega_0}{\Omega_{\rm w}}\sin\frac{\Omega_{\rm w}}{\Omega_0}\bar{t} \\ -\frac{\Omega_{\rm w}}{\Omega_0}\sin\frac{\Omega_{\rm w}}{\Omega_0}\bar{t} & \cos\frac{\Omega_{\rm w}}{\Omega_0}\bar{t} \end{pmatrix}, \tag{S20}$$

$$\bar{\mathbf{\Theta}}_{\rm D,WPP}(\bar{t}) = \frac{T\Gamma}{T_0\Omega_0} \begin{pmatrix} \bar{t}\frac{\Omega_0^2}{\Omega_{\rm w}^2}\left(1 - \operatorname{sinc} 2\frac{\Omega_{\rm w}}{\Omega_0}\bar{t}\right) & \frac{\Omega_0^2}{\Omega_{\rm w}^2}\sin^2\frac{\Omega_{\rm w}}{\Omega_0}\bar{t} \\ \frac{\Omega_0^2}{\Omega_{\rm w}^2}\sin^2\frac{\Omega_{\rm w}}{\Omega_0}\bar{t} & \bar{t}\left(1 + \operatorname{sinc} 2\frac{\Omega_{\rm w}}{\Omega_0}\bar{t}\right) \end{pmatrix}, \tag{S21}$$

$$\bar{\boldsymbol{u}}_{\rm WPP}(\bar{t}) = \bar{\Delta} \begin{pmatrix} 1 - \left(1 - \frac{\Gamma\bar{t}}{2\Omega_0}\right)\cos\frac{\Omega_{\rm w}}{\Omega_0}\bar{t} \\ -\left(1 - \frac{\Gamma\bar{t}}{2\Omega_0}\right)\frac{\Omega_{\rm w}}{\Omega_0}\sin\frac{\Omega_{\rm w}}{\Omega_0}\bar{t} \end{pmatrix}, \text{ where } \bar{\Delta} = \frac{F_{\rm c}}{m\Omega_{\rm w}^2}\sqrt{\frac{m\Omega_0^2}{k_{\rm B}T}}. \tag{S22}$$

It is clear that the case of $\Omega_{\rm w} = \Omega_0$ leads to the previously discussed case of the evolution in the PP.

Figure S1(c) demonstrates the effect of the application of the WPP. The original symmetric state (light gray) is extended in one direction and squeezed in the perpendicular one. During this process, the new elliptically-shaped state (dark gray) rotates with the frequency of $\Omega_{\rm w}$.

c. Inverted parabolic potential (IPP). The last potential that preserves the Gaussian shape of the particle's initial state is the IPP. Similar to the case of the WPP, applying this potential also leads to the extension and squeezing of the initial state in the phase space; however, the strength of the extension / squeezing is now, in principle, not limited. The strength of the operation again depends on the ratio of the characteristic frequencies of trapping (Ω_0) and inverted ($\Omega_{\rm i}$) potential and its evolution matrices are given by

$$\bar{\mathbf{U}}_{\rm IPP}(\bar{t}) = \begin{pmatrix} \cosh\frac{\Omega_{\rm i}}{\Omega_0}\bar{t} & \frac{\Omega_0}{\Omega_{\rm i}}\sinh\frac{\Omega_{\rm i}}{\Omega_0}\bar{t} \\ \frac{\Omega_{\rm i}}{\Omega_0}\sinh\frac{\Omega_{\rm i}}{\Omega_0}\bar{t} & \cosh\frac{\Omega_{\rm i}}{\Omega_0}\bar{t} \end{pmatrix}, \tag{S23}$$

$$\bar{\mathbf{\Theta}}_{\rm D,IPP}(\bar{t}) = \frac{T\Gamma}{T_0\Omega_0} \begin{pmatrix} \bar{t}\frac{\Omega_0^2}{\Omega_{\rm i}^2}\left(\frac{\Omega_0}{2\Omega_{\rm i}\bar{t}}\sinh 2\frac{\Omega_{\rm i}}{\Omega_0}\bar{t} - 1\right) & \frac{\Omega_0^2}{\Omega_{\rm i}^2}\sinh^2\frac{\Omega_{\rm i}}{\Omega_0}\bar{t} \\ \frac{\Omega_0^2}{\Omega_{\rm i}^2}\sinh^2\frac{\Omega_{\rm i}}{\Omega_0}\bar{t} & \bar{t}\left(1 + \frac{\Omega_0}{2\Omega_{\rm i}\bar{t}}\sinh 2\frac{\Omega_{\rm i}}{\Omega_0}\bar{t}\right) \end{pmatrix}, \tag{S24}$$

$$\bar{\boldsymbol{u}}_{\rm IPP}(\bar{t}) = \bar{\Delta}_{\rm i} \begin{pmatrix} \cosh\frac{\Omega_{\rm i}}{\Omega_0}\bar{t} - 1 \\ \frac{\Omega_{\rm i}}{\Omega_0}\sinh\frac{\Omega_{\rm i}}{\Omega_0}\bar{t} \end{pmatrix}, \text{ where } \bar{\Delta}_{\rm i} = \frac{F_{\rm c}}{m\Omega_{\rm i}^2}\sqrt{\frac{m\Omega_0^2}{k_{\rm B}T}}. \tag{S25}$$

In Eqs. (S23) and (S25), we completely omitted the damping factor Γ, as any damping is negligible compared to the exponential growth of the state in the unstable IPP.

Figure S1(d) shows the effect of the application of the IPP. The original symmetric state is expanded/squeezed, similarly to the previous case of the WPP. However, the principal axis of the squeezed state does not rotate, but rather approaches an asymptote line. In time, the expansion/squeezing grows exponentially with the rate $\sim \Omega_{\rm i}$.

S1.3. Characterization of variance of a general Gaussian state

It is useful to define quantities that characterize the deviation of a general evolving Gaussian state from the ideal thermal equilibrium (defined by the ambient temperature T) using the covariance matrix of the state. The covariance matrix uniquely defines an ellipse in the phase space having semi-axes of length $\bar{\sigma}_{\rm e}(\bar{t})$, $\bar{\sigma}_{\rm s}(\bar{t})$ and an angle $\varphi(\bar{t})$ between the longer semi-axis $\bar{\sigma}_{\rm e}(\bar{t})$ and the $\bar{z}$ axis. The lengths of these two semi-axes are given by the covariance matrix elements as

$$\bar{\sigma}_{\rm e,s}^2(\bar{t}) = \frac{1}{2}\left[\bar{\theta}_{zz}(\bar{t}) + \bar{\theta}_{vv}(\bar{t}) \pm \sqrt{\left(\bar{\theta}_{zz}(\bar{t}) - \bar{\theta}_{vv}(\bar{t})\right)^2 + 4\bar{\theta}_{zv}^2(\bar{t})}\right]. \tag{S26}$$

In the case of evolution in a harmonic optical trap (i.e., in the parabolic potential), the change of the semi-axes lengths in the limit $\Gamma \ll \Omega_0$, $\Gamma\bar{t}/\Omega_0 \ll 1$ can be expressed as

$$\begin{aligned} \bar{\sigma}_{\rm e,s}^2(\bar{t}) = & \frac{T\Gamma}{T_0\Omega_0}\bar{t} + \frac{(\bar{\theta}_{0zz} + \bar{\theta}_{0vv})}{2} \\ & \pm \frac{1}{2}\sqrt{\left(\bar{\theta}_{0zz} - \bar{\theta}_{0vv}\right)^2 + 4\bar{\theta}_{0zv}^2 + 4\frac{T\Gamma}{T_0\Omega_0}\left(\frac{T\Gamma}{T_0\Omega_0} - 2\bar{\theta}_{0zv}\right)\sin^2\bar{t} - 2\frac{T\Gamma}{T_0\Omega_0}\left(\bar{\theta}_{0zz} - \bar{\theta}_{0vv}\right)\sin 2\bar{t}}. \end{aligned} \tag{S27}$$

The term proportional to $T\Gamma/(T_0\Omega_0)$ is related to reheating (thermalization of the state). This term is responsible for the variation of the lengths of the semi-axes over time. Both $\bar{\sigma}_{\rm e}^2(\bar{t})$ and $\bar{\sigma}_{\rm s}^2(\bar{t})$ grow linearly in time in combination with their oscillations at $2\Omega_0$.

If the damping rate Γ can be neglected, as assumed above, the determinant of the covariance matrix remains constant and equal to 1 during the time evolution of the state. This means that the semi-axes satisfy $\bar{\sigma}_{\rm e}(\bar{t}) = 1/\bar{\sigma}_{\rm s}(\bar{t})$. Furthermore, it is useful to consider these parameters in the units of dB [8] as

$$\bar{\sigma}_{\rm s}(\bar{t})\ [\mathrm{dB}] = 10\log_{10}\bar{\sigma}_{\rm s}(\bar{t}), \tag{S28}$$

$$\bar{\sigma}_{\rm e}(\bar{t})\ [\mathrm{dB}] = 10\log_{10}\bar{\sigma}_{\rm e}(\bar{t}). \tag{S29}$$

On the logarithmic scale and with negligible damping rate, it holds $\bar{\sigma}_{\rm s}(\bar{t})\ [\mathrm{dB}] = -\bar{\sigma}_{\rm e}(\bar{t})\ [\mathrm{dB}]$.

S2. QUANTITATIVE TREATMENT OF DUFFING-TYPE NONLINEAR OSCILLATOR

In many types of nonlinear oscillators with a quasi-harmonic potential profile near the potential minimum, the nonlinearity only weakly modifies harmonic oscillations. In such a case, it is sufficient to add only the first nonlinear term to the description of the harmonic potential profile, given by a Taylor series expansion [9]. The so-called *Duffing oscillator* represents arguably the simplest physically relevant model of this type [9, 10]. On time scales shorter than any relevant thermalization, the motion of this oscillator can be described by the deterministic Duffing equation in the following form

$$\ddot{z} + \Gamma\dot{z} + \Omega_0^2 z\left(1 - \xi z^2\right) = 0. \tag{S30}$$

Compared to the previous definition of the forces in Eqs. (S3) and (S4), ξ represents the only additional parameter. It is called the coefficient of Duffing nonlinearity and is related to the third-order coefficient of the Taylor expansion of the optical force near the potential minimum at $z = 0$. Its existence appears quite naturally also in the classical case of the oscillating pendulum having the restoring force proportional to $\sin\varphi$, i.e. to the sine of the angle between vertical direction and the pendulum. Depending on the sign of the coefficient ξ, one may distinguish between the softening and hardening Duffing oscillator. In the definition adopted in Eq. (S30), $\xi > 0$ corresponds to the weakening Duffing force that will be the topic of our following analyses.

Using the perturbation analysis of such Duffing oscillator near $z = 0$ for weak damping, $\Gamma \ll \Omega_0$, leads to a solution in the form of damped oscillations [10]

$$z(t) = z_0 \exp\left(-\frac{1}{2}\Gamma t\right)\cos\left(\Omega_{\rm D} t + \delta_0\right), \tag{S31}$$

where z_0 and δ_0 are given by the initial conditions at $t = 0$. The frequency $\Omega_{\rm D}$ can then be expressed as [10]

$$\Omega_{\rm D}^2 = \Omega_0^2\left(1 - \frac{3}{4}\xi z_0^2\right) - \left(\frac{\Gamma}{2}\right)^2. \tag{S32}$$

Considering only weakly damped nonlinear oscillations, we can define the eigenfrequency of the damped quasi-harmonic oscillator Ω depending on its initial amplitude z_0 as [10]

$$\Omega = \sqrt{\Omega_{\rm D}^2 + (\Gamma/2)^2} \simeq \Omega_0\left(1 - \frac{3}{8}\xi z_0^2\right). \tag{S33}$$

For a nanoparticle optically confined in a standing wave (see next section for experimental details), the restoring optical force near the potential minimum follows

$$F \propto -\sin(2kz) \simeq -2kz[1 - (2kz)^2/6] \tag{S34}$$

to the third order, which is of interest in the present treatment. Upon comparison of Eq. (S34) with Eq. (S30), we obtain $\xi = (2k)^2/6$. Since it holds $\xi z^2 = \bar{\xi}\bar{z}^2$, we can use the definition of the dimensionless particle position (S9) to obtain the value of the dimensionless Duffing coefficient $\bar{\xi}$ as

$$\bar{\xi} = \frac{2}{3}\left(\frac{2\pi}{\lambda}\right)^2 \frac{k_{\rm B}T}{m\Omega_0^2}, \tag{S35}$$

where λ is the wavelength of the laser light used to generate the optical standing wave.

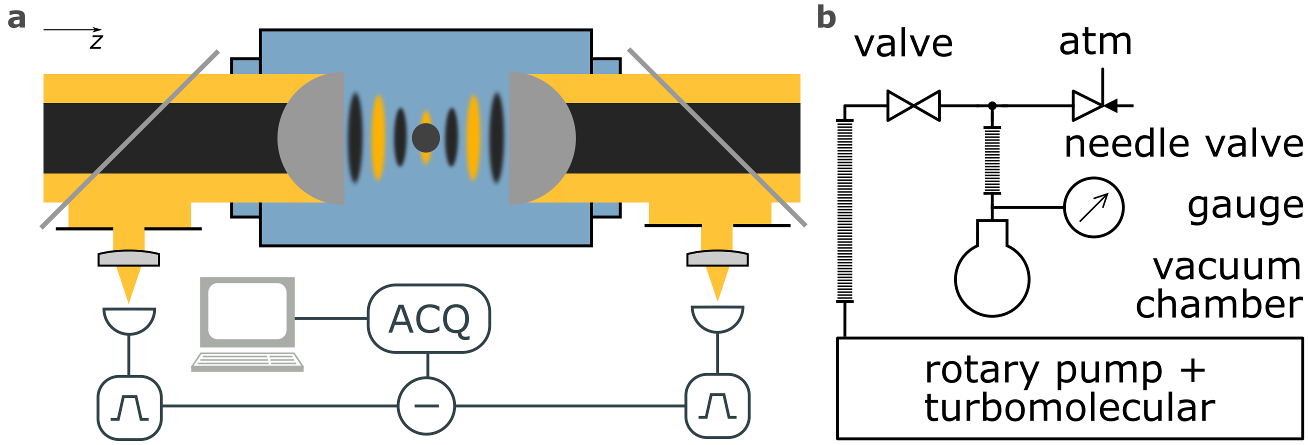

Figure S2. **Experimental geometry of the optical trapping and vacuum systems.** (a) Two counter-propagating interfering beams form a standing wave (SW; yellow) that serves as the primary optical trap and the nanoparticle levitates in its antinode. The nodes of a second SW formed by a pair of independent counter-propagating beams (black) nearly overlap with the anti-nodes of the primary trapping SW and provide an inverted parabolic potential. Both black and yellow SW can be switched on and off using acoustic-optical modulators (Fiber-Q® 1060 nm 150 MHz Hermetic Fiber-Coupled AOM) and they are frequency shifted by 300 MHz with respect to each other. This frequency difference, combined with asymmetries in the optical paths (right-hand versus left-hand paths), results in different positions of the nodes and antinodes of the two SWs; specifically, there is a mismatch $\Delta \approx 70\,\mathrm{nm}$ between the nodes of the black SW and the antinodes of the yellow SW. The particle's motion along the z-axis is detected by the reflection of $\approx 10\%$ of the trapping beams to the photodiodes of the balanced detector (Thorlabs PDB425C-AC). The blue region depicts the vacuum chamber. (b) Scheme of the vacuum system.

S3. EXPERIMENTAL CHARACTERIZATION OF NONLINEARITY OF THE OPTICAL TRAPPING POTENTIAL

The full description of the experimental setup and protocols can be found in [7]. A simplified scheme of the experimental setup is depicted in Fig. S2. The optical trap was configured as a standing wave created by two counter-propagating laser beams, each with a power of 20 mW and a wavelength $\lambda = 1064$ nm (Innolight Mephisto 2000NE), focused through a high numerical aperture lens (NA $= 0.77$). A spherical silica particle with a radius $a \approx 150\,\mathrm{nm}$ and density $\rho = 2000\,\mathrm{kg/m^3}$ was trapped in the intensity maximum of the standing wave, which had a beam waist of $\approx 1\,\mathrm{\mu m}$. To invert the optical trapping potential, we used an intensity minimum of a second, independent standing wave, which could be switched on and off independently on the primary trapping beam. This switching was achieved with acousto-optic modulators (AOMs), allowing us to change the optical potential within a fraction of the particle's oscillation period. All reported measurements were performed at 1 mbar. The position of the nanoparticle was detected using balanced shot-noise-limited detection along the optical axis (z). The mechanical oscillation frequency of the nanoparticle, $\omega/(2\pi) = 134.15\,\mathrm{kHz}$, was obtained by analyzing the power spectral density (PSD) of the levitated nanoparticle [11], see Fig. S3. Assuming these parameters of the experimental system and the ambient temperature of $T = 300$ K, the dimensionless Duffing coefficient calculated from Eq. (S35) was $\bar{\xi} = 4.8 \times 10^{-3}$.

The initial Gaussian state, defined by its mean values $\boldsymbol{\mu}_0$ and covariance matrix $\boldsymbol{\Theta}_0$ at $t = 0$, was modified using the potential pulses schematically illustrated in Fig. S1 and described in detail in [7]. While the minima of the WPP [Fig. S1(c)] and of the quasi-parabolic trapping potential overlapped, the maximum of the IPP [Fig. S1(d)] and the minimum of the quasi-parabolic trapping potential were mutually shifted by $\Delta \approx 70$ nm. As argued in [7], this subsequently led to an additional displacement of the state in the phase space, i.e., it shifted the mean values of the PDF away from the origin of the physical coordinates (z, v).

The particle was exposed to the WPP or IPP for a time τ_{w} or τ_{i}, respectively, which determined the extension/squeezing factors $\bar{\sigma}_{\mathrm{e}}(0), \bar{\sigma}_{\mathrm{s}}(0)$ of the initial Gaussian state (see Fig. S1(c,d) for illustration of squeezed Gaussian states). In this paper, the initial state at time $t = 0$ µs corresponds to the time instant immediately after applying the pulse of the WPP or IPP. However, in the experiments, we could correctly detect the nanoparticle position in the quasi-parabolic potential after the pulse only after the recovery time of the detection system ($\approx 3\,\mathrm{\mu s}$). This detection dead time was caused by the transient effects in the detection electronics induced by the abrupt changes of the incident photon flux during the stroboscopic protocol. To obtain the extension and squeezing factors $\bar{\sigma}_{\mathrm{e}}(0)$ and $\bar{\sigma}_{\mathrm{s}}(0)$ of the

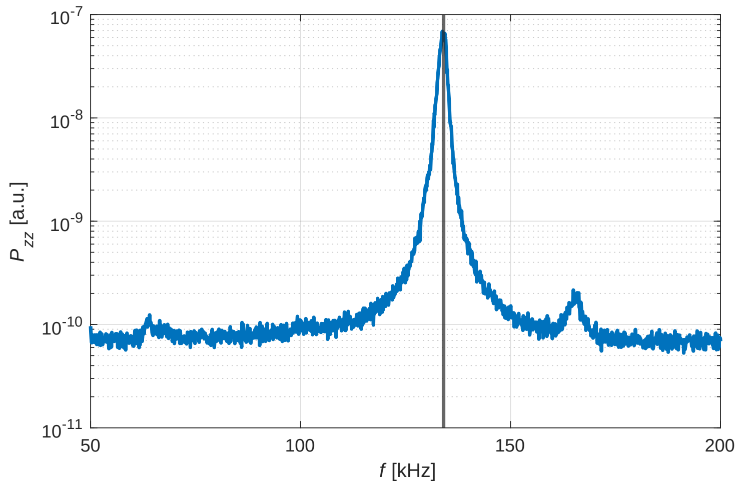

Figure S3. **Example of the power spectral density of particle position** obtained from a 1 s long record of the particle position. Vertical line shows the oscillation frequency, $f_{\rm PSD} \equiv \Omega_0/(2\pi) = 134.15$ kHz, used in the data processing and analysis.

initial Gaussian states that are reported in the main text, we applied model Eqs. (S16-S25) evaluated at time $\tau_{\rm w}$ or $\tau_{\rm i}$ to the thermal state that was experimentally characterized before subjecting the system to the corresponding WPP or IPP potential pulse (see also the leftmost panel of Fig. 1(b) of the main text and related discussion).

The WPP and IPP protocols were repeated independently multiple times (5000 each) while the nanoparticle position in the quasi-parabolic potential was detected with a sampling frequency of $\approx 10\,$MHz. The particle velocity was then calculated from the low-pass filtered position data as the second-order central difference of the positions. This way, statistical ensembles could be collected, allowing us to reconstruct the particle motional state using the procedures detailed in [7].

S4. REGULARIZATION IN THE ESTIMATION OF PARAMETERS OF FERMAT'S SPIRAL-BASED COORDINATES

In the discussion of coordinate transformations presented in the main text, we state that regularization [12] is necessary in order to properly estimate the parameters $(a, \Phi_{\rm s}, \bar{\rho}_0)$ defining the coordinate system based on the displaced Fermat's spiral (FS), which is described by Eqs. (10) of the main text:

$$\bar{r}_{\rm s} = \sqrt{\bar{e}_{\rm s}^2 + \bar{\rho}_0^2}, \tag{S36}$$

$$\varphi_{\rm s} = \Phi_{\rm s} + \operatorname{atan}\frac{\bar{e}_{\rm s}}{\bar{\rho}_0} + a(\bar{e}_{\rm s}^2 + \bar{\rho}_0^2). \tag{S37}$$

The optimal parameters of the FS coordinates can be found using Eq. (12) of the main text

$$(a, \Phi_{\rm s}, \bar{\rho}_0) = \operatorname{argmin}\left[\operatorname{var}\left(\bar{s}_{\rm s}\right) + \lambda_{\rm R} L(a, \Phi_{\rm s}, \bar{\rho}_0)\right], \tag{S38}$$

where the variance of the squeezed variable $\bar{s}_{\rm s}$ is calculated over the ensemble of all experimental data points $(\bar{z}_m, \bar{v}_m)$ included in the state upon their transformation from the physical phase space to the FS-based coordinates using Eqs. (10) and (11) of the main text. For the given set $(a, \Phi_{\rm s}, \bar{\rho}_0)$, the values of $\bar{s}_{\rm s}$ are given by

$$\bar{s}_{\rm s} = \min_{\bar{e}_{\rm s}}\left[\bar{r}_{\rm m}^2 + \bar{e}_{\rm s}^2 + \bar{\rho}_0^2 - 2\bar{r}_{\rm m}\sqrt{\bar{e}_{\rm s}^2 + \bar{\rho}_0^2}\cos\left(\phi_{\rm m} - \Phi_{\rm s} - \operatorname{atan}\frac{\bar{e}_{\rm s}}{\bar{\rho}_0} - a(\bar{e}_{\rm s}^2 + \bar{\rho}_0^2)\right)\right]^{\frac{1}{2}}, \tag{S39}$$

with $\bar{r}_{\rm m}^2 = \bar{z}_{\rm m}^2 + \bar{v}_{\rm m}^2$, $\phi_{\rm m} = \operatorname{atan}(\bar{v}_{\rm m}/\bar{z}_{\rm m})$, and the length $L(a, \Phi_{\rm s}, \bar{\rho}_0)$ of the FS spiral is

$$L(a, \Phi_{\rm s}, \bar{\rho}_0) = \int_{\bar{e}_{\rm s1}}^{\bar{e}_{\rm s2}} \sqrt{\left(\frac{{\rm d}\bar{r}_{\rm s}}{{\rm d}\bar{e}_{\rm s}}\right)^2 + \bar{r}_{\rm s}^2\left(\frac{{\rm d}\varphi_{\rm s}}{{\rm d}\bar{e}_{\rm s}}\right)^2}\,{\rm d}\bar{e}_{\rm s} = \int_{\bar{e}_{\rm s1}}^{\bar{e}_{\rm s2}} \sqrt{1 + 4a\bar{e}_{\rm s}\bar{\rho}_0 + 4a^2\bar{e}_{\rm s}^2\left(\bar{e}_{\rm s}^2 + \bar{\rho}_0^2\right)}\,{\rm d}\bar{e}_{\rm s}, \tag{S40}$$

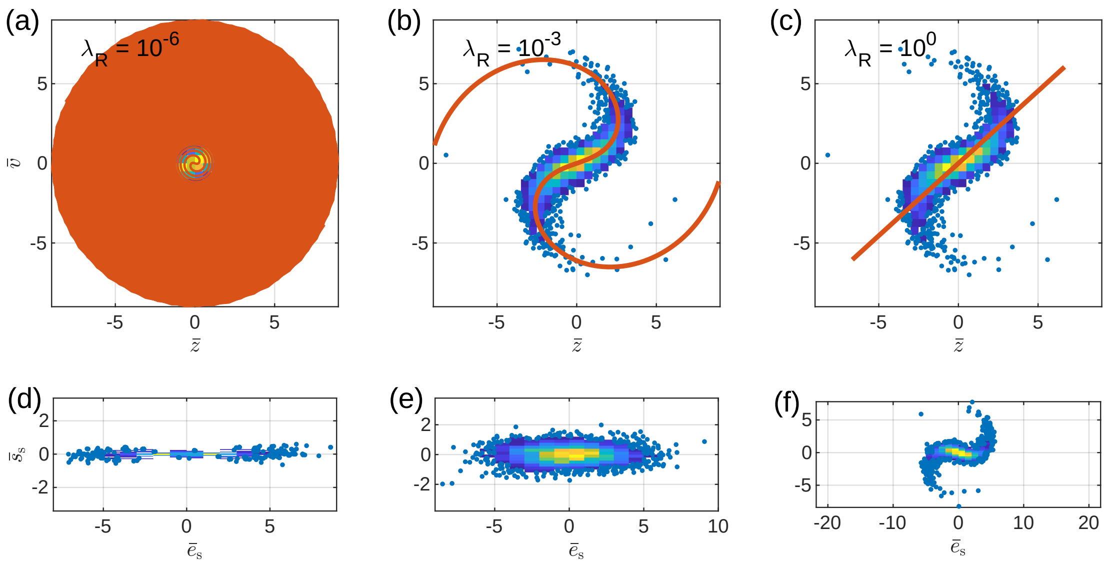

Figure S4. **Influence of the regularization strength λ_R on the parameters of the FS-based coordinate system.** Red curves in panels (a-c) depict the shape of the curvilinear $\bar{e}_s$-axis, superimposed on the experimental state PDF recorded at time $\bar{t} = 4\pi$ (i.e., after 2 periods of transient evolution) and expressed in the physical phase-space coordinates $(\bar{z}, \bar{v})$. Panels (d-f) show the corresponding state PDFs in the FS-based curvilinear coordinates $(\bar{e}_s,\ \bar{s}_s)$ with the parameters obtained by minimization using the regularization strengths displayed in (a-c).

with the integration limits $\bar{e}_{s1,2}$ being the extremal extended coordinates $\bar{e}_s$ of the experimental state realization.

The regularization strength λ_R in Eq. (S38) controls the relative influence of the spiral length, L, over the minimized variance, var $\bar{s}_s$, of the squeezed variable in the minimization process, penalizing longer spirals. In effect, this selectively restricts the accessible space of the FS parameters $(a, \Phi_s, \bar{\rho}_0)$ and in doing so, it significantly improves the overall stability of the parameter estimation process [13]. Figure S4 shows three examples of FS-based coordinate systems obtained for the values of $\lambda_R = 10^{-6}$, 10^{-3}, and 1. In all three cases, the parameters of the FS-based spiral coordinates were evaluated at dimensionless time $\bar{t} = 4\pi$, i.e. after 2 periods of transient evolution of the initial squeezed state in a quasi-parabolic potential, for experimental parameters specified in Section S3. Figures S4(a-c) show the experimentally recorded state PDF in the physical phase-space coordinates $(\bar{z}, \bar{v})$ with superimposed FSs depicting the $\bar{e}_s$ axis ($\bar{s}_s = 0$) of the new FS-based coordinate system. For a weak regularization considered in part a ($\lambda_R = 10^{-6}$), the spiral winds extremely fast, which leads to a negligible variance of the variable $\bar{s}_s$ upon the coordinate transformation. This is directly illustrated in Fig. S4(d), which shows the reconstructed state PDF in the $(\bar{e}_s,\ \bar{s}_s)$ coordinates. However, it is obvious that the corresponding FS obtained from the minimization represents poorly the actual contour of the experimental PDF. Figure S4(b) shows the proper FS-based coordinate system found for the regularization strength $\lambda_R = 10^{-3}$, with the corresponding Gaussian-like state PDF in the curvilinear coordinates $(\bar{e}_s,\ \bar{s}_s)$ shown in Fig. S4(e). For this particular value of λ_R, the FS found in the minimization process correctly follows the shape of the experimentally observed state PDF. Finally, Fig. S4(c) shows the state transformation with a strong regularization, $\lambda_R = 1$. Here, the spiral length constraint dominates in the minimized function (S38), effectively forbidding fast-winding spirals. Consequently, this results in a nearly-Cartesian coordinate system rotated with respect to the original physical coordinates, compare Fig. S4(c,f).

The choice of the optimal value of λ_R is guided by the actual experimental data and by independent physically grounded assumptions about their boundedness [13, 14]. As a rule of thumb, the practical choice follows

$$1 < \frac{\lambda_R L(a, \Phi_s, \bar{\rho}_0)}{\text{var } (\bar{s}_s)} < 10. \tag{S41}$$

For our particular data, Eq. (S41) yields $\lambda_R \sim 10^{-3}$, which is the value used to obtain the FS-based coordinates shown in Fig. S4(b,e) and in the main text.

[1] J. Millen, T. S. Monteiro, R. Pettit, and A. N. Vamivakas, Optomechanics with levitated particles, Reports on Progress in Physics **83**, 026401 (2020).

[2] W. Paul, Electromagnetic traps for charged and neutral particles, Reviews of Modern Physics **62**, 531 (1990).

[3] T. Li, S. Kheifets, and M. G. Raizen, Millikelvin cooling of an optically trapped microsphere in vacuum, Nature Physics **7**, 527 (2011).

[4] S. A. Beresnev, V. G. Chernyak, and G. A. Fomyagin, Motion of a spherical particle in a rarefied gas. Part 2. Drag and thermal polarization, Journal of Fluid Mechanics **219**, 405 (1990).

[5] H. Risken, *The Fokker-Planck Equation* (Springer-Verlag, Berlin, 1996).

[6] S. Chandrasekhar, Stochastic Problems in Physics and Astronomy, Reviews of Modern Physics **15**, 1 (1943).

[7] M. Duchaň, M. Šiler, P. Jákl, O. Brzobohatý, A. Rakhubovsky, R. Filip, and P. Zemánek, Nanomechanical state amplifier based on optical inverted pendulum, Communications Physics **8**, 276 (2025).

[8] M. Rashid, T. Tufarelli, J. Bateman, J. Vovrosh, D. Hempston, M. S. Kim, and H. Ulbricht, Experimental Realization of a Thermal Squeezed State of Levitated Optomechanics, Physical Review Letters **117**, 273601 (2016).

[9] S. Strogatz, *Nonlinear Dynamics and Chaos with Applications to Physics, Biology, Chemistry and Engineering* (Westview Press, Boulder, 2015).

[10] I. Kovacic and M. J. Brennan, *The Duffing Equation: Nonlinear Oscillators and their Behaviour* (John Wiley & Sons, Ltd., 2011).

[11] E. Hebestreit, M. Frimmer, R. Reimann, C. Dellago, F. Ricci, and L. Novotny, Calibration and energy measurement of optically levitated nanoparticle sensors, Review of Scientific Instruments **89**, 033111 (2018).

[12] A. N. Tikhonov, A. V. Goncharsky, V. V. Stepanov, and A. G. Yagola, *Numerical Methods for the Solution of Ill-Posed Problems* (Springer Netherlands, Dordrecht, 1995).

[13] A. E. Hoerl and R. W. Kennard, Ridge Regression: Biased Estimation for Nonorthogonal Problems, Technometrics **12**, 55 (1970).

[14] G. H. Golub, M. Heath, and G. Wahba, Generalized Cross-Validation as a Method for Choosing a Good Ridge Parameter, Technometrics **21**, 215 (1979).